PERGAMON

Scripta mater. 44 (2001) 2729–2734

Scripta MATERIALIA

www.elsevier.com/locate/scriptamat

INFLUENCES OF OXIDE PHASES ON THE COERCIVITY OF MECHANICALLY ALLOYED MULTICOMPONENT Fe-BASED AMORPHOUS ALLOYS

Y.J. Liu[1], I.T.H. Chang[2] and M.R. Lees[3]

[1]Department of Materials Engineering, University of Wales Swansea, Singleton Park, Swansea, SA2 8PP, UK [2]School of Metallurgy and Materials, The University of Birmingham, Edgbaston, Birmingham, B15 2TT, UK [3]Department of Physics, University of Warwick, Coventry, CV4 7AL, UK

(Received November 15, 2000)
(Accepted January 9, 2001)

Keywords: Mechanical alloying; Metallic glasses; Oxidation; Coercivity

Introduction

Recently, it has been reported that an almost fully amorphous phase can be obtained by mechanically alloying of the Fe-based multicomponent alloy systems [1,2]. However, the mechanically alloyed amorphous Fe-based alloys exhibit a higher coercivity than the melt-spun counterparts with similar chemical compositions. One of major causes of such a high coercivity may be the presence of oxide phases in the amorphous alloy, e.g. Al_2O_3 in Fe-Al-P-C-B alloy [1] and B_2O_3, ZrO_2 in Fe-Co-Ni-Zr-B alloys [2]. In the present study, the amorphous alloy powders were subjected to in-situ annealing inside a vibration sample magnetometer (VSM) and a transmission electron microscope (TEM) in order to investigate the effects of oxide particles on coercivity of the as-milled amorphous alloy powders during annealing.

Experimental Methods

A Fritsch P5 planetary ball mill was used to perform the mechanical alloying of powders. The milling speed was set at 0.675m/s. The ball-to-powder weight ratio was maintained at 25 for each run. The environmental temperature inside the milling pot was kept as low as possible. An air-cooling fan was running constantly to cool the pots during the milling process. The starting materials were elemental metal powders of Fe, Co, Ni, B and prealloyed $Zr_{70}Ni_{30}$ (wt.%) powders with purities above 99.5%. The initial powder particle size varied from 25 to 120 microns for various powders. 10 grams of metal powders with 250 grams hardened stainless balls of 4 mm in diameter were loaded together into the milling pot inside a glove bag, which was first evacuated and then back-filled with purified argon. An O-ring seal was seated between the milling pot and the lid. This was used to prevent any possible migration of oxygen into the milling pot from the surrounding atmosphere during ball milling. The amorphous phase was obtained by milling the starting powders for 18 hours. For in-situ heating in the TEM, the powders were encapsulated in a Ni matrix using a standard nickel plating process [3]. Metal powders were pressed onto a tin surface to form the cathode, and a pure nickel plate was used as an

PII: S1359-6462(01)00962-9

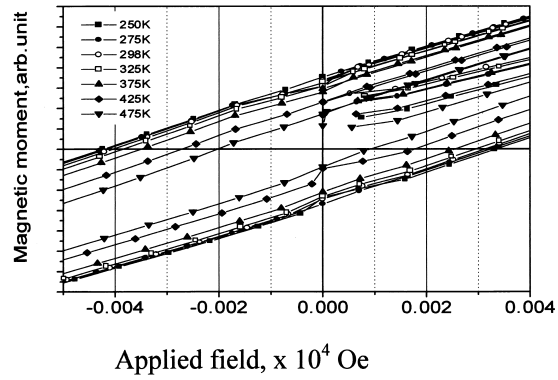

Figure 1. M-H loops for the as-milled alloy powders annealed at a range of temperatures between 250 and 475K; (a) $Fe_{56}Ni_{14}Zr_{10}B_{20}$, (b) $Fe_{49}Ni_{21}Zr_{10}B_{20}$ and (c) $Fe_{42}C0_7Ni_{21}Zr_{10}B_{20}$.

anode. The Ni plating was performed at a current of 200mA and a voltage of 2–3 V. Disc specimens of 3 mm in diameter were punched off from the Ni plated sheet of the composite sample, and dimpled down to a thickness of about 40–50 microns. Ion beam thinning was performed to obtain a perforation at the centre of the specimen. In-situ heating experiments in the TEM were carried out in a Philips FX4000 at 400kV. The coercivity of the amorphous powders was measured in Oxford Maglab VSM in the temperature range between room temperature and 575K in magnetic fields of up to 1 T (i.e. 10000Oe).

Results and Discussion

Figure 1 shows typical M-H loops of $Fe_{56}Ni_{14}Zr_{10}B_{20}$ annealed at various temperatures ranging from 250 to 475K. Similar measurements were carried out for $Fe_{49}Ni_{21}Zr_{10}B_{20}$ and $Fe_{42}Co_7Ni_{21}Zr_{10}B_{20}$ alloys. The coercivity was determined from these M-H loops. These measured coercivity was plotted against the annealing temperature for various as-milled amorphous alloy powders, as shown in Figure 2. The coercivity at room temperature ranges from 36 to 42 Oe. This is slightly higher than that for the as-milled Fe-Al-P-C-B amorphous alloy (28 Oe, Schlorke, 1999). The coercivity (H_{ci}) of the as-milled powders was significantly reduced with increasing annealing temperature. For $Fe_{56}Ni_{14}Zr_{10}B_{20}$ alloys, the coercivity decreased steadily with increasing temperature from 250 to 575K. However, for

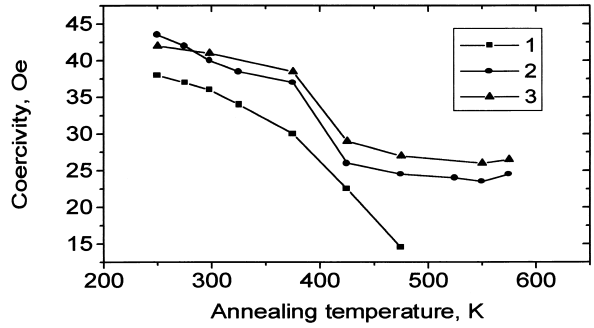

Figure 2. Annealing temperature dependence of coercivity of as-milled powders of 1.$Fe_{56}Ni_{14}Zr_{10}B_{20}$, 2. $Fe_{49}Ni_{21}Zr_{10}B_{20}$, 3. $Fe_{42}Co_7Ni_{21}Zr_{10}B_{20}$.

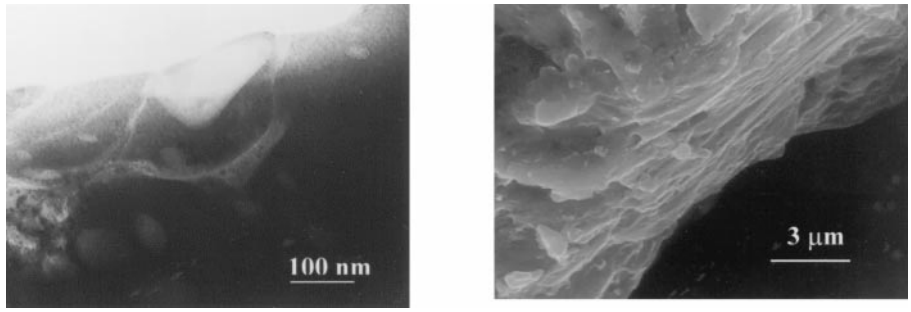

Figure 3. A bright field TEM image (left) and a secondary electron SEM micrograph (right) showing the internal imperfect interfaces between the keying powders and the external multilayered structure, respectively.

$Fe_{49}Ni_{21}Zr_{10}B_{20}$ and $Fe_{42}Co_7Ni_{21}Zr_{10}B_{20}$ alloys, the coercivity decreased initially with temperature and then gradually reached a minimum value at temperatures above 400K. In addition, the coercivities for $Fe_{49}Ni_{21}Zr_{10}B_{20}$ and $Fe_{42}Co_7Ni_{21}Zr_{10}B_{20}$ alloys were found to be generally higher than that for $Fe_{56}Ni_{14}Zr_{10}B_{20}$ alloy. Obviously, the coercivities of the amorphous powders in both as-milled and as-annealed states are much higher than that of the melt-spun amorphous alloys or that of the as-annealed FeAlPCB amorphous alloy (Hci = 170A/m, or 2.1Oe) made by MA [2].

The high coercivity found in mechanically alloyed soft magnetic powders may be caused by the several factors: internal stress, special domain structure and/or the presence of non-magnetic oxides.

The effect of the internal stress is briefly analysed here. In the late stages of the milling process, the amorphous powders are flattened and deformed by colliding media. The flattened surface may experience a much higher strain rate deformation than the core. Since there is a limited plastic strain in the amorphous powder, the impact load from the colliding balls may not transfer into the core. This may induce a variation in the residual stress across the flattened amorphous powder. Consequently, the residual stress on the surface of the flattened powder is likely to be compressive. Furthermore, the flattened amorphous powders with different degrees of deformation are mechanically keyed together but without sufficient time for the atomic diffusion to complete between them. This results in the formation of imperfect interfaces between the flattened amorphous powders. Finally, a multi-layered structure is developed in the resultant MAed amorphous powder. The internal and the external multi-layered features have been observed by TEM and SEM, respectively, as shown in Figure 3. These imperfect interfaces may act as pinning sites for domain walls and may cause an increase in H_{ci}.

The maximum coercivity that could be caused by internal stress is generally estimated to be about 10 Oe for magnetic materials [4]. The internal stress present in the as-milled alloy powder may be released to a certain degree by annealing but this may also lead to an undesired change in the required microstructure at high temperatures. For example, the annealing of the as-milled nanostructured Fe-Zr-B-Cu powder at 660°C for 15 minutes cannot completely remove the internal stress but does cause grain growth. Thus, the coercivity is only reduced by a factor of two by annealing at elevated temperatures without significant grain growth [5]. In the present case, the crystallisation temperatures of the as-milled Fe-Ni(Co)-Zr-B alloy powders are close to 600K [2] which is not sufficient to remove the internal stress in the as-milled alloy powder completely without any crystallisation. In addition, the presence of oxide phases created during MA or during annealing of the amorphous powders may lead to a high coercivity. The coercivity H_{ci} of MAed amorphous $Fe_{56}Ni_{14}Zr_{10}B_{20}$ with some amount of boron oxide particles, has been reduced by 80% through the annealing at the temperatures without any crystallisation of amorphous phase. However, the coercivities of the other two MAed amorphous alloys (e.g. $Fe_{49}Ni_{21}Zr_{10}B_{20}$ and $Fe_{42}Co_7Ni_{21}Zr_{10}B_{20}$) can only be reduced by 30–40% by annealing. This is due to the co-existence of the B_2O_3 and ZrO_2 oxide particles as reported by Liu [6]. The B_2O_3 particles

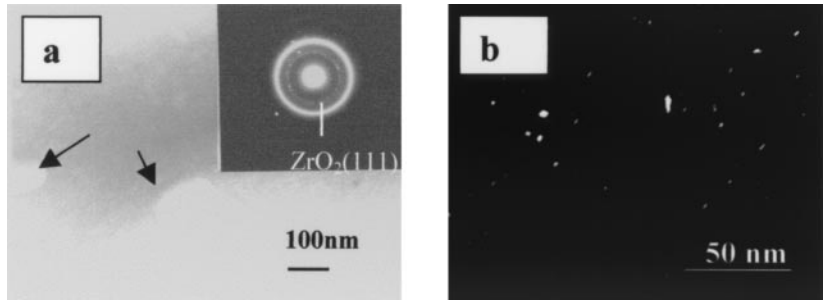

Figure 4. (a) A TEM bright field image and the corresponding SADP showing the amorphous phase and B_2O_3 particles (as indicated by arrows), (b) a dark field TEM image showing the presence of ZrO_2 particles in the as-milled $Fe_{49}Ni_{21}Zr_{10}B_{20}$ alloy powder.

were produced due to the reaction of remaining boron during MA. The ZrO_2 oxide particles were produced either during MA of the $Fe_{49}Ni_{21}Zr_{10}B_{20}$ or during the annealing of the $Fe_{42}Co_7Ni_{21}Zr_{10}B_{20}$ amorphous powders. Figure 4a shows a bright field TEM micrograph and a corresponding selected area diffraction pattern (SADP) of the as-milled $Fe_{49}Ni_{21}Zr_{10}B_{20}$ alloy powder. It is clear that the B_2O_3 particles are present in the amorphous phase matrix. In addition, there is a broken fine ring inside the halo ring in SADP suggesting the presence of ZrO_2 oxide particles in the amorphous matrix. Figure 4b gives the dark field TEM image of the ZrO_2 particles with a higher magnification. The size and the area fraction of the ZrO_2 particles can be estimated to be 1–10nm and 1.5%, respectively. The size and the area fraction of the B_2O_3 particles can be estimated to be 30–80nm and 3–5% respectively. In contrast, Figures 5a and 5b, show that no ZrO_2 oxide phase was detected and only a few B_2O_3 particles were found in the matrix phase of the as-milled $Fe_{56}Ni_{14}Zr_{10}B_{20}$, and $Fe_{42}Co_7Ni_{21}Zr_{10}B_{20}$ alloys. The sizes and the volume fractions of B_2O_3 present in $Fe_{56}Ni_{14}Zr_{10}B_{20}$ are 20–100nm and 5% respectively. However, the size of B_2O_3 was reduced to 20–30nm while the volume fraction of B_2O_3 was 4% for $Fe_{42}Co_7Ni_{21}Zr_{10}B_{20}$. The ZrO_2 oxide particles may be produced by an oxygen-triggered reaction during the annealing of the $Fe_{42}Co_7Ni_{21}Zr_{10}B_{20}$ amorphous powders. This has been confirmed by in-situ heating amorphous powder in the TEM, as shown in Figure 6. Thus, the minimum Hci value of the as-annealed $Fe_{42}Co_7Ni_{21}Zr_{10}B_{20}$ amorphous powders in Figure 2 may be due to this oxygen-triggered reaction of zirconium element.

Control of the oxygen impurities in as-milled alloy powders has been an important issue for MA because the presence of any oxygen in the amorphous alloys may lead to a deterioration in the thermal and magnetic properties. Fiedler [7] has suggested that a small amount of nonmagnetic particles such

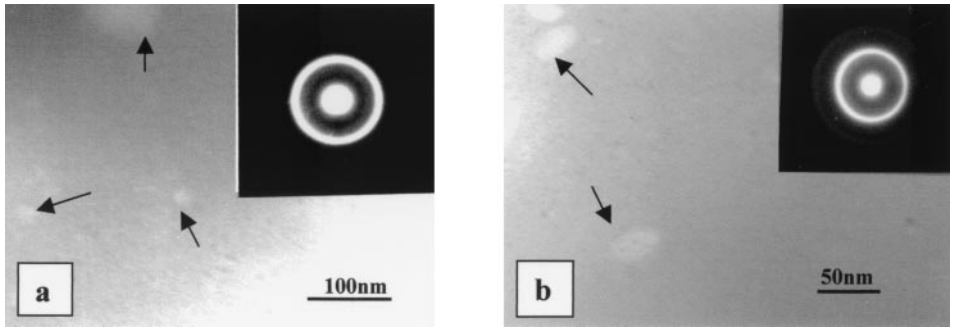

Figure 5. TEM bright field images showing the amorphous matrix and B_2O_3 particles (as indicated by arrows) in (a) $Fe_{56}Ni_{14}Zr_{10}B_{20}$ and (b) in $Fe_{42}Co_7Ni_{21}Zr_{10}B_{20}$ as-milled powders.

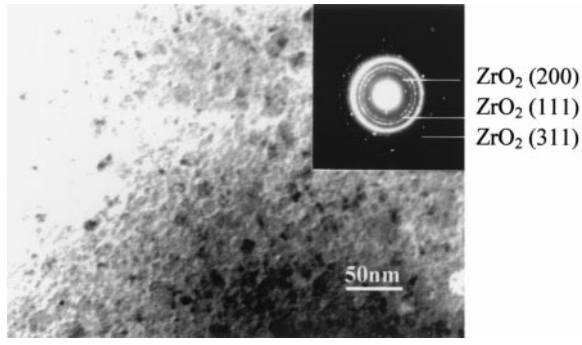

Figure 6. Bright field TEM micrographs and the corresponding SAD patterns of as-milled $Fe_{42}Co_7Ni_{21}Zr_{10}B_{20}$ alloy powders after in-situ heating at 523K for 30 minutes.

as oxides may be the reason for an increase in coercivity. This can be explained by the ′inclusion theory′ [8] and the disperse field theory [9]. Generally, a change in domain wall energy occurs when the wall intersects one or more of these inclusion particles. The intersection of the domain wall with inclusions reduces the domain area and this leads to a decrease in the energy of the domain wall. However, if a random distribution of the imperfect inclusions is considered, the wall energy variation should be very small. In this case, the disperse field theory should better explain the inclusion effect on coercivity. When the size of inclusions is below a certain critical value (comparable to the wall thickness, δ), free poles form around the inclusions; For larger inclusions, Neel spikes form. The effect of fine ZrO_2 and B_2O_3 oxide particles in the as-annealed amorphous powders may be roughly estimated using Neel′s formula provided the strain effect is negligible in the as-annealed amorphous powder.

$$H_{ci} \approx 360\ v' \tag{1}$$

Where v′ is the fractional volume of non-magnetic inclusions.

The contribution of B_2O_3 to coercivity takes a constant value because the volume fraction is constant during annealing of the amorphous powder. For an average volume fraction of B_2O_3 of 4% for all the alloys investigated, the H_{ci} contributed by B_2O_3 is about 14.4 Oe using equation (1). The contribution of ZrO_2 to coercivity is dependent on annealing temperature. If its average volume fraction is taken as 1.5%, then the H_{ci} caused by ZrO_2 should be approximately 5.4 Oe. Therefore, the overall contribution of B_2O_3 and ZrO_2 to H_{ci} may be up to19.8 Oe.

Conclusion

The high coercivity of the mechanically alloyed amorphous powders is mainly caused by the internal stress and oxide phases. The coercivity can be significantly reduced by annealing of as-milled amorphous powder at temperatures below T_g due to the release of internal stress. However, the portion of H_{ci} contributed by oxide phases cannot be removed by annealing. The oxidation of the as-milled powders during the annealing prevents the H_{ci} from decreasing further. The contributions of residual stress, B_2O_3 and ZrO_2 to H_{ci} can be analysed semi-quantitively using Neel′s formula.

Acknowledgments

The authors would like to thank Prof. I. R. Harris for the provision of experimental facilities at the School of Metallurgy and Materials, The University of Birmingham. Y. J. Liu is very grateful to the ORS award for the financial support.

References

1. N. Schlorke, J. Eckert, and L. Schultz, J. Phys. D. Appl. Phys. 32, 855 (1999).
2. Y. J. Liu, I. T. H. Chang, and P. Bowen, J. Mater. Sci. Eng. A. Special issue for RQ10 (2000).
3. C. J. Smithells, Metals Reference Book, 5th edn., p. 1496, Butterworths, London (1976).
4. A. H. Morrish, the Physical Principles of Magnetism, p. 389, John Wiley & Sons, New York (1965).
5. R. Schafer, S. Roth, C. Stiller, J. Eckeet, U. Klement, and L. Schultz, IEEE Trans. Magn. 32, 4383 (1996).
6. Y. Liu, Ph.D. Thesis, The University of Birmingham (2000).
7. H. C. Fielder, J. D. Livingston, and S. C. Huang, J. Magn. Magn. Mater. 26, 157 (1981).
8. A. H. Morrish, The Physical Principles of Magnetism, p. 390, John Wiley & Sons, Inc., New York (1965).
9. R. Carey and E. D. Isaac, in Magnetic Domains and Techniques for Their Observation, p. 37, English Universities Press (1966).